ISSN 1330-3651 (Print), ISSN 1848-6339 (Online)
Received: 14 June 2025; Accepted: 26 August 2025

https://doi.org/10.17559/TV-20250614002749
Original scientific paper

Modified Antlion Optimization Based Voltage Control for Five Level Packed U Cell Inverter in Grid Integrated Photovoltaic Charging System for Electric Vehicles

S. RAMYA*, G. SUNDAR

Abstract: The transportation and energy sectors are increasingly integrating electric vehicles (EVs) as essential components of sustainable development. Photovoltaic (PV)-powered charging stations, comprising PV modules interfaced with the public grid, offer a reliable and cost-effective solution for EV battery charging. However, these stations typically introduce nonlinear loads, leading to significant current distortions that degrade power quality. To mitigate these issues, Shunt Active Power Filters (SAPFs) are employed to suppress harmonic currents and ensure clean energy delivery. The inverter in the SAPF operates as a controlled current source, injecting compensating harmonics in parallel with the nonlinear load. A key component in this system is the DC link voltage controller, which directly influences the accuracy of harmonic compensation. This study proposes a Modified Antlion Optimization Algorithm (MALO) for DC link voltage control in a SAPF using a Five-Level Packed U Cell (PUC5) inverter for a grid-connected PV system with EV charging capabilities. The MALO algorithm surpasses ALO in terms of convergence rate and circumvents the local optima. MALO optimises the parameter of the PI controller in SAPF using the objective function of integral time absolute error (ITAE). The performance of the MALO-based controller is compared against a Particle Swarm Optimization (PSO) approach under identical system configurations. Both models are evaluated using MATLAB/Simulink simulations based on a modified instantaneous reactive power (MIRP) theory for harmonic current extraction. Results demonstrate that the MALO-based control achieves superior harmonic mitigation, reducing Total Harmonic Distortion (THD) to as low as 1.53%, thereby outperforming the PSO-based system. Maximum harmonic compensation of around 96.75% is achieved with the help of the proposed system compared to uncompensated power system. The findings validate the effectiveness of MALO for improving power quality in PV-powered EV charging infrastructures.

Keywords: electric vehicle charging; harmonic mitigation; modified antlion optimization; puc5 multilevel inverter; shunt active power filter

1 INTRODUCTION

Power distribution networks need to make provision for the novel and unusual load that electric vehicle (EV) chargers represent [1]. Non-linear loads, such as electric vehicle chargers, have the potential to cause problems with distribution feeder power quality (PQ), which could lead to a reduction in equipment longevity. Consumers, equipment makers, and utility corporations are becoming very concerned about power quality. Harmonic pollution, another name for the issue with harmonics in the electrical grid, is not a recent occurrence. A number of disruptions in the electrical network are brought about by non-linear loads that are linked to the grid. These loads consume non-sinusoidal currents and produce harmonic distortion. At different grid connection sites, these current harmonics will produce harmonic voltages in turn [2, 3]. The SAPF has been chosen from a variety of potential solutions for harmonic minimization. The harmonic elements of nonlinear loads are cancelled out using SAPFs, which function in shunt across the source and the nonlinear load. Various SAPF topologies have been presented, with an emphasis on harmonic identification techniques and component characteristics [4, 5].

The utilisation of multilevel inverter topologies is on the rise because of their superior electromagnetic compatibility, high power, superior waveform quality, and reduced switching losses [6]. Several types of multilevel inverters and their uses in filtering are covered in a survey and comparison research [7-10]. Packed U-cell (PUC) inverters have several benefits over standard multilevel inverters, including fewer devices [11], less complicated regulation, as well as greater power quality [12]. Therefore, in order to increase power quality for SAPF, a modified five-level PUC inverter is suggested in this article.

The SAPF's DC-link control is crucial to the system's power quality. Regrettably, the PI-traditional controller - which employs the pole placement approach, the Routh-Hurwitz criterion, the Root locus method, or the Ziegler-Nichols (ZN) tuning formula are not adaptable to changes in the parameters of non-linear systems. Furthermore, the majority of these methods were unable to optimise the parameters for this classical controller. Therefore, for on-line self-tuning adaptive PI controllers, evolutionary computing and intelligent approaches like genetic algorithms (GA), PSO, bacteria-foraging optimisation, ant-colony optimisation, and artificial bee colonies are increasingly applied [13-17]. The Modified Grey Wolf Optimizer (MGWO) is employed in [18] to optimise power flow correction for wind turbine induction generators by adjusting and achieving optimal settings for a PI controller. Optimising the PI-controller variables (Kp and Ki) in order to treasure the optimal solution in the search space is the aim of the optimisation process.

An examined power quality enhancement [19] by ant colony optimisation (ACO) based SAPF, demonstrates enhanced performance via comparative study with PI and Adaptive Neuro-Fuzzy Inference System (ANFIS) using numerous types of algorithms, including firefly optimisation (FO), PSO, harmony search optimisation (HSO), and predator-prey based firefly optimisation (PPFO) algorithms, an examined current THD reduction with the aid of SAPF. It is evident that PPFO provided the highest compensation compared to the other algorithms. Simultaneously, it also confirms the enhanced efficacy of FO and PPFO compared to ACO in harmonic mitigation [20].

An optimisation method called the Ant Lion Optimizer was created in [21] to address a variety of actual engineering issues. It mimics nature's antlion hunting method. Seven popular and contemporary algorithms from the literature were compared to the ALO algorithm: PSO and GA, States of Matter Search (SMS), Flower Pollination Algorithm (FPA), Bat Algorithm (BA), CuckooSearch (CS) algorithm, and FO. The suggested algorithm beats other approaches in a broad range of test

functions and yields highly desirable results, according to the results in [21]. The survey states that ALO is capable of performing better than PSO, GA, SMS, BA, FPA, CS, and FO optimisation algorithms.

A harmonic reduction utilising GWO and ALO-based SAPF, found that ALO outperformed GWO in harmonic compensation [22]. Nevertheless, for certain optimisation issues, the ALO algorithm experiences poor convergence speed and local optima stagnation. Hence this article suggests a modified antlion optimisation (MALO) technique that modifies the antlion position while accumulating a new parameter based on each ant's step length to enrich the primary ALO performance.

As per literature [23] MALO algorithm increases Accuracy rate, Balanced Accuracy (BACC) rate, Geometric mean (G-mean) rate and Area Under the Curve (AUC) for "Breast _tissue" dataset, over other algorithms such as ALO, GWO and Whale Optimization Algorithm (WOA) as shown in Tab. 1.

Table 1 Comparative performance of MALO with other optimisation algorithms

Parameter	Increment in (%) by MALO than		
	ALO	GWO	WOA
average g-mean	6.14	10.53	20.22
average accuracy	3.08	9.23	8.46
average bacc	3.85	3.85	11.54
average auc	5.56	8.17	16.67

Meanwhile, research [23] claims that, similar to the "Breast _tissue" dataset, the MALO algorithm outperformed ALO, GWO, and WOA on at least 10 of the 15 datasets tested. Hence in this research MALO proposed for DC link voltage control in SAPF.

This study formulates the analysis of SAPF as an optimisation problem with many goals, including enhancing DC-link voltage control, for minimizing the THD of the source current by maintaining it at the reference value. A couple of optimisation techniques, PSO and MALO, are used to tackle the problem. In this study, overshoot, settling time, and DC-link voltage ripples are considered vital objectives. Comparing PI-MALO to the PI-PSO-based SAPF, simulation results demonstrate a significant increase in harmonic mitigation.

Motivation, novelty and principal contributions of this work:

- The motivation for selecting this problem is to design a swarm intelligence technique such as the PSO algorithm and MALO. The MALO algorithm escapes local optima and provides a better convergence rate, so it eliminates the inaccuracies involved in the conventional PI and other optimisation algorithms.
- The DC link controller (PI) parameters are tuned using the PSO algorithm and MALO. The controller parameters are tuned using the objective function of ITAE. The algorithm minimises the objective function.
- The MALO-tuned PI for SAPF with PUC5 inverter was not analysed by earlier research.

2 PROPOSED SYSTEM

This study analyses a grid-connected solar power system that supplies an electric vehicle charging station with SAPF for harmonic reduction, as depicted in Fig. 1. A photovoltaic power system consists of a grid-connected inverter, conditioner, and PV array. A PV power system's conditioner controls voltage and tracks maximum power. The PV voltage is adequate for grid integration thanks to the inverter. PV and grid-supplied electric vehicle charging stations are included in this research.

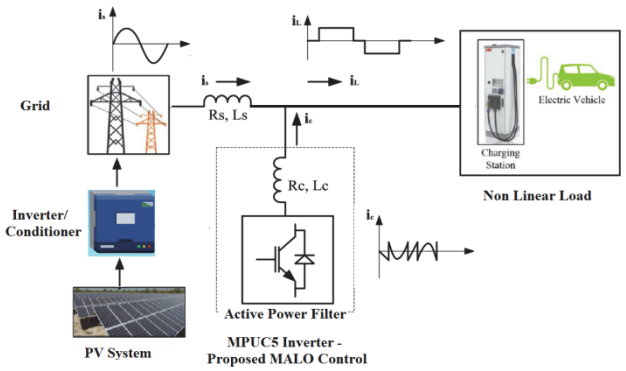

Figure 1 Proposed hybrid power system with SAPF

EV charging station is perfect nonlinear load for grid makes unpredictable and huge harmonics in the grid. SAPF between grid and charging station injects compensation signal for harmonic mitigation.

Active filters are used to solve the problem of harmonics with voltage and current [24]. This research investigates the utilisation of SAPF to effectively tackle the current harmonics issues. The structure of a self-controlled dc bus SAPF is like a static compensator, utilised in transmission systems to regulate reactive power. Fig. 1 depicts a simple schematic of a SAPF. It can be noted that a SAPF acts as a source of current by injecting the harmonic element of the load current, however with a 180° phase shift. An AC motor driven by a voltage source PWM inverter is one example of a nonlinear load. Whether using or not using a transformer, the load producing harmonics is linked in parallel to the SAPF.

The SAPF block diagram (Fig. 1) depicts a voltage fed converter with a PWM current controller and a SAPF controller. The controller continuously senses the instantaneous load current (IL). The controller now separates the harmonic element from the load current using a low pass filter. Controlling the filter current is mostly dependent on the ac inductor L of the diode rectifier, which is situated on the ac side. SAPF can provide reactive power balance alongside harmonic correction.

$\tilde{p}\&\tilde{q}$ are the values of the positive sequence elements that make up the IL, while $\tilde{p}\&\tilde{q}$ are the values of the harmonic elements of the load current. SAPF has been configured to get the reactive power portion of the whole q and the AC portion of real power p for reactive power and harmonic mitigation in order to determine the optimal reference current. As shown in Eq. (1), the instantaneous real power equivalent to the loss element of the SAPF (p_{loss}) is additionally incorporated into the ac element of real power ($-\tilde{p}$), in order to reimburse for the inverter losses of the SAPF.

$$\begin{bmatrix} i_{c\alpha}^{*} \\ i_{c\beta}^{*} \end{bmatrix} = \begin{bmatrix} v_{\alpha} v_{\beta} \\ -v_{\beta} v_{\alpha} \end{bmatrix}^{-1} \begin{bmatrix} -\tilde{p} + p_{\text{loss}} \\ -q \end{bmatrix} \tag{1}$$

Inverse Clarke's transform is used for transforming these currents back to a-b-c coordinates, as shown in Eq. (2).

$$\begin{bmatrix} i_{ca}^{*} \\ i_{cb}^{*} \\ i_{cc}^{*} \end{bmatrix} = \sqrt{\frac{2}{3}} \begin{bmatrix} 1 & 0 \\ -\frac{1}{2} & \frac{\sqrt{3}}{2} \\ -\frac{1}{2} & -\frac{\sqrt{3}}{2} \end{bmatrix} \begin{bmatrix} i_{c\alpha}^{*} \\ i_{c\beta}^{*} \end{bmatrix} \tag{2}$$

The triggering pulses are created by a hysteresis band regulator, and the produced reference current is compared against the measured filter currents. The PI controller receives the variance amid the DC link voltage (V_{dc}) and its reference (V_{ref}) to generate p_{loss}. As shown in Fig. 2, the actual setup of a SAPF necessitates voltage control at the inverter DC end (V_{dc} - the capacitor voltage), wherein a reference voltage V_{ref} is required for an active filter inverter to operate suitably.

For power computations, devoid of distortion voltage readings have to be collected to maximise the effectiveness of the SAPF under less-than-ideal grid voltage scenarios. Fig. 2 illustrates how the grid voltages can be filtered using a low pass filter. Formerly filtering, the voltages are transmuted into synchronous reference frame to facilitate the removal of voltage imbalances.

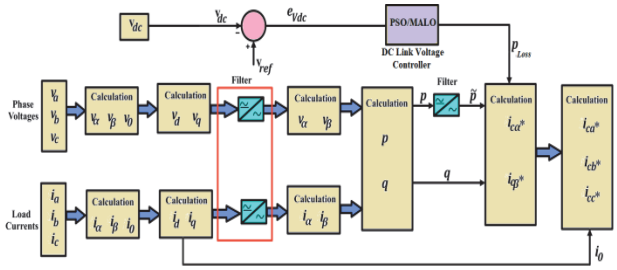

Figure 2 Block diagram of modified *p-q* theory

The change into the synchronous reference frame is discussed below.

$$\begin{bmatrix} v_d \\ v_q \end{bmatrix} = \begin{bmatrix} cos\,\phi & -sin\,\phi \\ sin\,\phi & cos\,\phi \end{bmatrix} \begin{bmatrix} v_\alpha \\ v_\beta \end{bmatrix} \tag{3}$$

PUC 5 level inverter

A PUC inverter configuration usually entails a pair of DC lines and six semiconductor switching elements, all working together seamlessly. There are three interrelated pairs of switches [12]. Each pair contains a few switches that work well together. Every set of active devices is linked to a DC connection, forming a U-Cell. The PUC inverter consists of U-Cells. There is a dc capacitor positioned on the underside of the inverter, while a DC supply is situated on the top side as one of the two DC links. The voltage of the dc capacitor is regulated through the use of a switching technique. The rating disparity between the highest-ranked two switches and the remaining four switches is exactly half. This is the outcome of voltage stress on the switches. Unlike the lower pairs of switches, which can only handle the capacitor voltage or VDC/2, the top pairs of switches need to endure a voltage identical to the supplied DC voltage. Fig. 3 displays a PUC5 inverter with three phases.

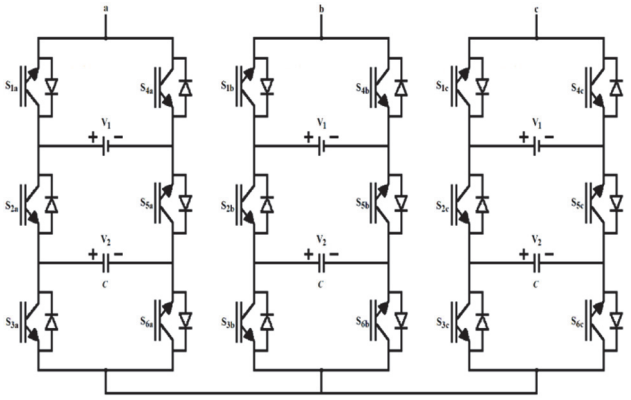

Figure 3 Three phase PUC5 inverter

There are a variety of feasible switching states for the PUC inverter, which are displayed in Tab. 2.

Table 2 Triggering of PUC inverter

Possible states	S_1	S_2	S_3	Output Voltage	V_{load}	Capacitor Voltage
1	ON	OFF	OFF	V_1	$2V$	No effect
2	ON	OFF	ON	$V_1 - V_2$	V	Charging
3	ON	ON	OFF	V_2	V	Discharging
4	ON	ON	ON	0	0	No effect
5	OFF	OFF	OFF	0	0	No effect
6	OFF	OFF	ON	$-V_2$	$-V$	Discharging
7	OFF	ON	OFF	$V_2 - V_1$	$-V$	Charging
8	OFF	ON	ON	$-V_1$	$-2V$	No effect

Tab. 2 shows that every different switching state offers a distinct pathway for current to flow to the load. Varying voltage levels are produced through numerous switching states. As a function of DC link amplitude, the number of operational voltage levels is defined. According to Tab. 2, there can be at the utmost 7 output voltage levels. In order to achieve a voltage output with seven levels, it is necessary for the capacitor voltage to be 1/3 of VDC. The seven output voltage levels resulting from the given assumptions are 0, ±V, ±2V, and ±3V. The intricate voltage balancing mechanism of the 7-level PUC inverter is responsible for its numerous drawbacks. Operating the device in 5-level voltage output mode can help overcome the drawbacks of the seven-level PUC inverter. By precisely managing the capacitor voltage at half of the DC supply voltage, it is possible to create a 5 level PUC inverter. The voltage output can be represented by five levels: 0, ±V, and ±2V. This assumes that VDC is equal to 2VC, which is equal to 2V. Tab. I shows that there are some duplicate states, as a couple of switching states produces a null voltage and 4 switching states produce –V and +V. Through the process of charging and discharging a DC capacitor, it becomes possible to effectively control the voltage of the capacitor to half of the DC source voltage. Utilising the multicarrier PWM approach, superfluous states are employed. The proposed PUC5 configuration of SAPF utilises only 18 switching devices, which is a lower quantity compared to what is required for a cascaded 5-level inverter.

DC link controller

The two primary functions of the DC side capacitor are to sustain a steady state DC voltage and to provide actual power differential between the source and load during the transient phase by acting as an energy storage component. Every time the load varies, the voltage of the DC link capacitor varies as well. Utilising a controller, the desired controlled voltage is obtained. While the PI controller is employed in traditional systems, our analysis suggests tuning the PI controller to improve MALO and PSO performance.

Problem Formulation and Objective Function

The coefficients of the PI controller KP and Ki are obtained in this work using the MALO and PSO. Eradicating the harmonic currents produced by the nonlinear load in the electrical grid is the primary goal of the optimal PI controller design. The cost function that needs to be minimised is the Integral of Time Average Error (ITAE). The following is the objective function.

$$J = 2 \cdot M_p + \int t \cdot \left| e(t) \right| \mathrm{d}t \tag{4}$$

where (e) represents the error as determined by the subsequent Eq. (5) and (J) represents the cost function

$$e = V_{\mathrm{dcref}} - V_{\mathrm{dc}} \tag{5}$$

Consequently, the subsequent optimisation issue can be used to formulate the design problem: The proposed technique minimises the overall harmonic distortion by using MALO and PSO to find the ideal set of PI controller coefficients.

Particle Swarm Optimization

In its global variant, the PSO method starts with a population of possible stochastic solutions, which are perceived as particles travelling around the search space. Because of its speed and short memory, each of the nearby particles under consideration is able to recall its optimal performance in terms of both positioning and value. Every particle's performance is evaluated in accordance with a predetermined goal function associated with the issue that needs to be resolved [25]. Each particle's velocity at cycle (k + 1) is a function of its position and velocity at cycle k, as well as the disparity between its present position and its best overall and previous positions, respectively.

Phase-by-phase PSO Algorithm

The PSO algorithm is represented by the subsequent steps:

Phase 1: To meet the inequality criteria, establish an array of particles with arbitrary locations and corresponding velocities.

Phase 2: Verify that the quality constraints are satisfied, and adjust the solution as needed.

Phase 3: Assess each particle's fitness function.

Phase 4: Contrast the particle's prior best value (pbest) with the fitness function's current value. Provide the current coordinates (positions) to pbestx if the present fitness value is less.

Phase 5: Among the present places, get the present global minimum fitness value.

Phase 6: Evaluate the global minimum of currently (gbest) with the global minimum of yesterday. Allocate the present global least to gbest and the present coordinates (positions) to gbestx if the current global lowest is superior to gbest.

Phase 7: Adjust the velocities in accordance with Eq. (6).

$$\begin{aligned} v_i^{k+1} &= W v_i^k + c_1 rand_1 (pbest_i + S_i^k) + \\ &+ \ c_2 rand_2 (gbest_i + S_i^k) \end{aligned} \tag{6}$$

where: $c_{1,2}$: acceleration- factors; *gbest*: the best member of the group; $pbest_i$: agent i's *pbest*; *rand*: a random number that ranges from 0 to 1; S_i^k : agent i's present position at cycle k; V_i^k : the agent's velocity at cycle k; W: the function of weighting.

Phase 8: After moving every particle to its new location in accordance with Eq. (7), go back to Phase (2).

$$S_i^{k+1} = S_i^k + V_i^{k+1} \tag{7}$$

where S_i^{k+1}: new present position of agent i at cycle k + 1; V_i^{k+1} : new velocity of agent i at cycle k + 1.

Phase 9: Till anending condition is met or the maximum number of cycles is achieved, repeat Phases 2 to 8. In this analysis c_1 and c_2 = 2, number of particles = 15 and maximum iterations = 100.

AntlionOptimizer

In 2015, Seyedali Mirjalili introduced the Antlion Optimizer (ALO), which draws inspiration from the foraging process of lions and ants [21]. The five main processes in this foraging approach are the random walk (RW) of agents, trapping ants in the trap, establishing traps, reestablishing traps, and catching prey. The ALO algorithm tracks the interactions between ants and antlions.

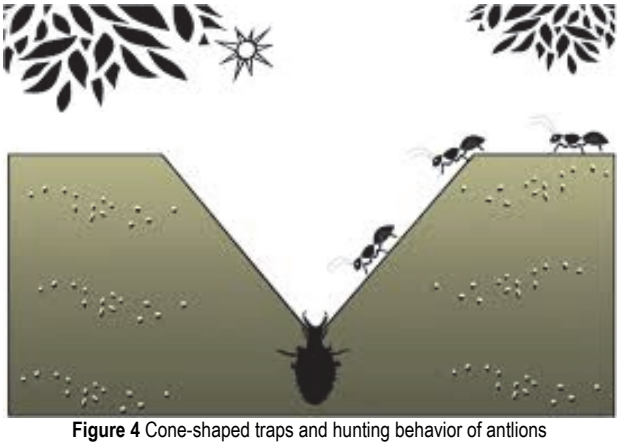

Figure 4 Cone-shaped traps and hunting behavior of antlions

Antlions rely on traps, as seen in Fig. 4, to entice the ants, and ants are allowed to arbitrarily drift into the search area in search of food.

The matrices that depict the locations of p ants and p antlions are shown below; q is the quantity of variables (dimension).

$$S_{Ant} = \begin{bmatrix} Ant_{1,1} & Ant_{1,2} & \ldots. & Ant_{1,q} \\ Ant_{2,1} & Ant_{2,2} & \ldots. & Ant_{2,q} \\ \ldots. & \ldots.. & \ldots. & \ldots\ldots.. \\ Ant_{p,1} & Ant_{p,2} & \ldots. & Ant_{p,q} \end{bmatrix} \tag{8}$$

$$S_{Antlion} = \begin{bmatrix} Antlion_{1,1} & Antlion_{1,2} & \ldots. & Antlion_{1,q} \\ Antlion_{2,1} & Antlion_{2,2} & \ldots. & Antlion_{2,q} \\ \ldots. & \ldots.. & \ldots. & \ldots\ldots.. \\ Antlion_{p,1} & Antlion_{p,2} & \ldots. & Antlion_{p,q} \end{bmatrix} \quad (9)$$

The matrices generated the matrices for conserving the fitness value (objective) of p ants (S_{OAnt}) and p antlions ($S_{OAntlion}$) if f represented a function of fitness for the length of optimisation.

$$S_{OAnt} = \begin{bmatrix} f([\,Ant_{1,1} & Ant_{1,2} & \ldots. & Ant_{1,q}\,]) \\ f(\left[\,Ant_{2,1} \right. & Ant_{2,2} & \ldots. & \left. Ant_{2,q}\,\right]) \\ \ldots. & \ldots.. & \ldots. & \ldots\ldots.. \\ f(\left[\,Ant_{p,1} \right. & Ant_{p,2} & \ldots. & \left. Ant_{p,q}\,\right]) \end{bmatrix} \quad (10)$$

$$S_{OAntlion} = \begin{bmatrix} f([\,Antlion_{1,1} & Antlion_{1,2} & \ldots. & Antlion_{1,q}\,]) \\ f([\,Antlion_{2,1} & Antlion_{2,2} & \ldots. & Antlion_{2,q}\,]) \\ \ldots. & \ldots.. & \ldots. & \ldots\ldots.. \\ f([\,Antlion_{p,1} & Antlion_{p,2} & \ldots. & Antlion_{p,q}\,]) \end{bmatrix} \quad (11)$$

There are six operators in the ALO algorithm.

(i) RW of Ants. Ants use a random walk $X(t)$ to update their positions at each and every optimisation stage. Eq. (12) is used for determining a random walk. The present reiterate, or iteration, is denoted by t, the cumulative sum is calculated by cumsum, the greatest number of iterations is T, and rand suggests an arbitrary number utilising the uniform distribution of probabilities with an interval [0, 1].

$$X(t) = 0, \text{cumsum}\left(2r(t_1)-1\right), \text{cumsum}\left(2r(t_2)-1\right), \ldots.., \text{cumsum}\left(2r(t_T)-1\right) \quad (12)$$

where the statistic function $r(t)$ is illustrated as in Eq. (13).

$$r(t) = \begin{cases} 1 \text{if } rand > 0.5 \\ 0 \text{if } rand \le 0.5 \end{cases} \quad (13)$$

Since each search region has a boundary to keep the random walks in the search zone, the ants are normalised. Before updating the ant position, Eq. (14) is applied to normalise the procedure using the accompanying equation (minmax normalisation). Whereas ai is the ith variable's lowest random walk, q_i is its greatest random walk; c_i^t denotes the ith variable's lowest at the tth repetition, and q_i^t denotes the ith variable's maximum at the tth iteration.

$$X_i^t = \frac{(X_i^t - a_i) \times (q_i - C_i^t)}{(q_i^t - a_i)} + c_i^t \quad (14)$$

(ii) Trapping in Antlion's Pits. Ants' RWs are impacted by Antlion's traps. The c and q vectors across a selected antlion reflect the ant's RW in a hypersphere, as shown by Eqs. (15) and (16). The lowermost total variable at the t^{th} cycle is implied by lc^t in these equations; the uppermost total variable at the t^{th} cycle is suggested by the vector hq^t; the lowermost total variable for the i^{th} ant is implied by c_i^t; the uppermost total variable for the i^{th} ant is indicated by q_i^t; and the place of the chosen j^{th} antlion of the tth cycle is indicated by $Antlion_j^t$ where i is the existing ant's index and j denotes the current antlion's index.

$$c_i^t = Antlion_j^t + lc^t \quad (15)$$

$$q_i^t = Antlion_j^t + hq^t \quad (16)$$

(iii) Building Trap. In the ALO technique, a roulette wheel active to choose the fitter antlions meant to capture ants depends on the fitness value for the duration of optimisation.

(iv) Sliding Ants towards Antlion. Antlions have the ability to construct traps in a proportional manner, while ants exhibit random modifications that correspond to their fitness values.

Once the ants are inside the trap in the centre of the pit, antlions spray sand outward. The imprisoned ant, which is trying to escape the trap, is slid down by this performance; in this case, the ants' random walk hypersphere's range is adjusted. Taking into account that rc^t and rq^t represent the condensed vectors of the total variables' lowermost and uppermost random walks at the t^{th} cycle, correspondingly:

$$rc^t = \frac{lc^t}{I} \quad (17)$$

$$rq^t = \frac{hq^t}{I} \quad (18)$$

The vector hq^t recommends incorporating the vector of the greatest total variables at the tth cycle whereas lc^t implies the least of all variables at that cycle. I also indicates a ratio that was determined as follows:

$$I = 10^{\omega}\left(t/T\right) \quad (19)$$

where w represents a fixed quantity centred on the current repetition t. Typically, the constant value w may handle the intensity of movement and accuracy.

The Eqs. (17) and (18) replicate the sliding motion of an ant into the pits and reduce the range of the modifying ants' locations.

(v) Capturing Targets and Re-establishing the Pit. As soon as the ant goes to the lowermost of the pit, it is captured by the antlion. To rise its probabilities of capturing newly discovered prey, the antlion updates its place based on the tracked ant's most recent circumstances, as shown in Eq. (20):

$$Antlion_j^t = Ant_i^t if\ f\left(Antlion_j^t\right) < f\left(Ant_i^t\right) \tag{20}$$

where the location of the selected jth antlion at the t^{th} repetition was expressed by $Antlion_j^t$, and the position of the i^{th} ant at the t^{th} iteration is implied by Ant_i^t.

(vi) Elitism. Elitism is a crucial component of the evolutionary method that maintains the best explanation or clarifications found at each stage of the optimisation process. In the MALO process, the best antlion is an elite. By including an extra parameter Tu that is dependent on the step length for every ant and updating the antlion position depending on the parameter Tu, the higher and lower boundaries of the search space, MALO is presented as a way of enhancing the optimisation precision and efficacy of ALO [23].

$$Tu = \frac{i}{p} \tag{20}$$

$$mu = 10\left(Tu \times 100\right) \tag{21}$$

$$yt = 2 \times rand \times \left(\text{size}\left(R_A^t\right)\right) - 1 \tag{22}$$

$$dx = \frac{\left(1+mu\right)\cdot abs\left(yt\right) - 1}{mu \times sign\left(yt\right) \times \left(ub - lb\right)} \tag{23}$$

In the ALO process, the best antlion is an elite. As stated in Eq. (24), every single ant RW across a deliberately certain antlion via the roulette wheel and the elite immediately.

$$Ant_i^t = \left(\frac{R_A^t + R_E^t}{2}\right) \Big/ dx \tag{24}$$

In this expression, the roulette wheel selects the random walk denoted by R_A^t throughout the antlion at the tth repetition, and R_E^t implies the RW throughout the elite at the same repetition.

Consider X to be the function that generates the random primary outcomes; Y controls the initial population that function X presents; Z returns to true while the termination principle is guaranteed. The ALO process can be recognised as a three-tuple using the previously suggested operations, as seen below:

$$ALO\left(X, Y, Z\right) \tag{25}$$

where the functions X, Y, and Z are expressed as below

$$\varnothing \xrightarrow{X} \left\{S_{Ant}, S_{OAnt}, S_{Antlion}, S_{OAntlion}\right\} \tag{26}$$

$$\left\{S_{Ant}, S_{Antlion}\right\} \xrightarrow{Y} \left\{S_{Ant}, S_{Antlion}\right\} \tag{27}$$

$$\left\{S_{Ant}, S_{Antlion}\right\} \xrightarrow{Z} \left\{\text{true, false}\right\} \tag{28}$$

Here, S_{Ant} denotes the ant's location matrix, $S_{Antlion}$ includes the antlions' location, S_{OAnt} contains the ant's ensuing fitness, and $S_{OAntlion}$ contains the antlions' fitness. In this analysis Number of search agents ants and antlions is set as 40 and maximum iteration is 10.

4 SIMULATION RESULTS AND ANALYSIS

The power system with SAPF is examined using MATLAB/Simulink with a focus on analysis. A 60kw photovoltaic power system is employed to supply a nonlinear load to the grid. The system under analysis is characterised by a three-phase, 410 V, 50 Hz, and 100 kW load. Fig. 5 illustrates the function of the photovoltaic system under standard thermal conditions (STC).

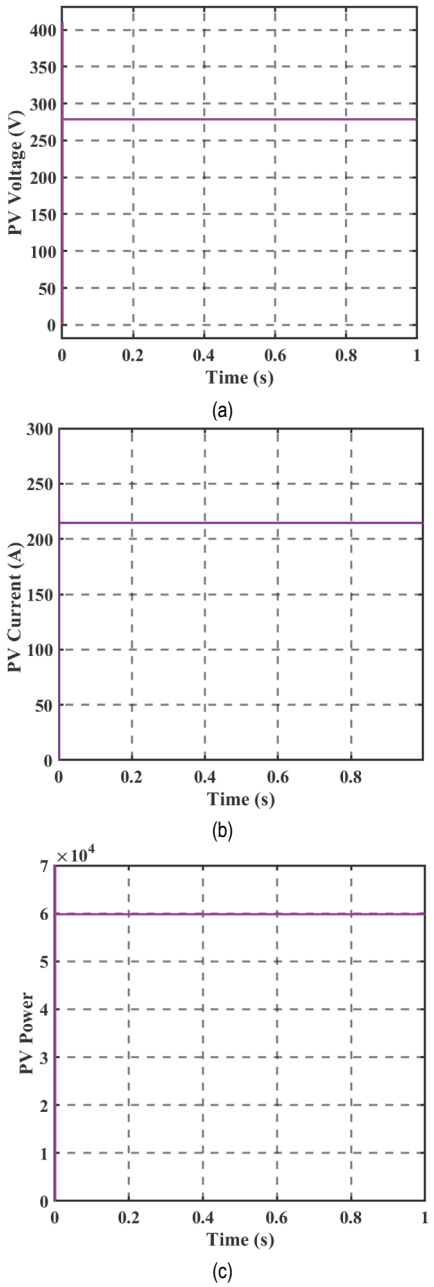

Figure 5 Operation of PV system under STC (a) Voltage; (b) Current; (c) Power

Based on the Fig. 5, it can be noticed that the STC PV system displays a maximum power output of 60 kW, accompanied by an ultimate voltage of 275 V and the highest possible current of 218.18 A. Fig. 6 illustrates the performance of a power system when subjected to a nonlinear load.

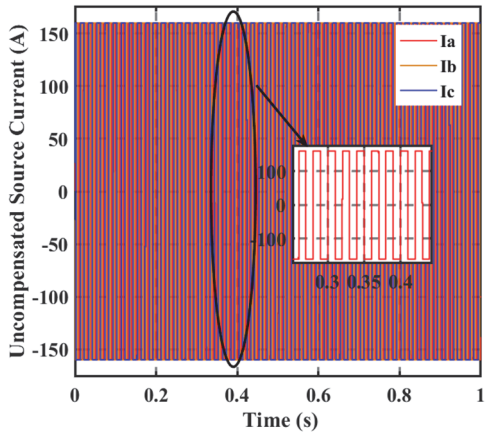

(a)

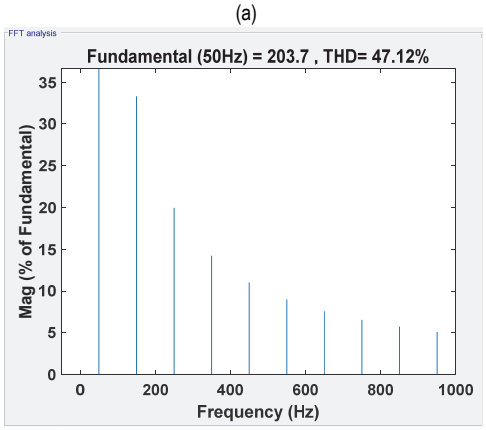

(b)

Figure 6 Operation of power system with nonlinear load without filter (a) Source current; (b) THD in source current

EV charging facilities result in notable source current variations, as Fig. 6 demonstrates. EV impact modifies the shape of the source current, resulting in high harmonics of 47.12%.

Under nonlinear load, the performance of PUC5 inverter based SAPF is investigated utilizing PSO and MALO tuned PI based DC link controller. Performance of PUC5 inverter based SAPF utilizing PSO tuned PI based DC link controller is shown in Fig. 7.

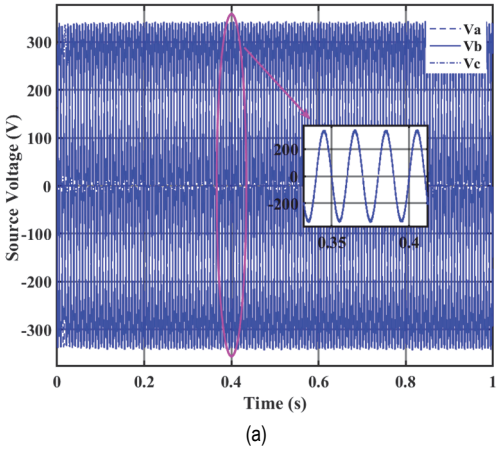

(a)

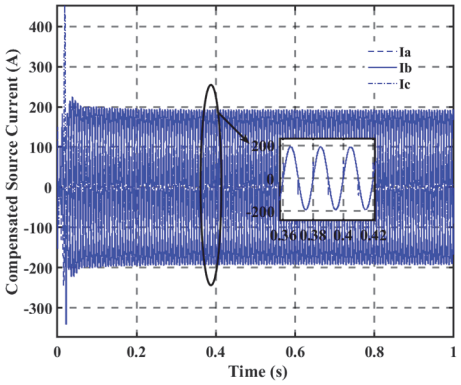

(b)

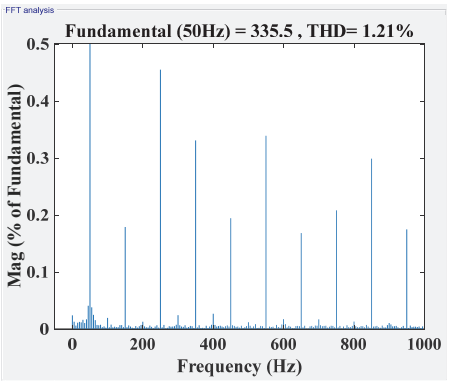

(c)

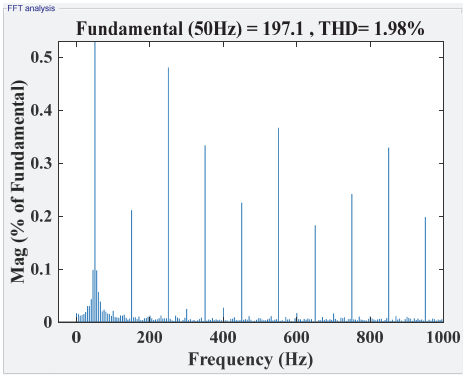

(d)

Figure 7 Operation of PSO based SAPF with PUC5 inverter (a) VSabc; (b) ISabc; (c) THDV; (d) THDi

It is clear from Fig. 7 that using PSO controlled SAPF improves the source current's form. The THDi is 1.98% and the THDV is 1.21%, as shown in Fig. 7, both of which are below 5% of the IEEE norm. The performance of a SAPF with PUC5 inverter using the suggested MALO-based DC link controller is presented in Fig. 8.

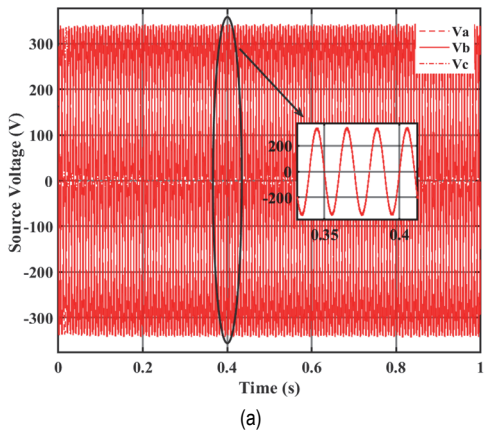

(a)

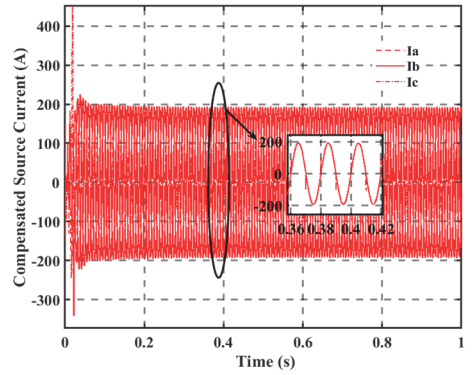

(b)

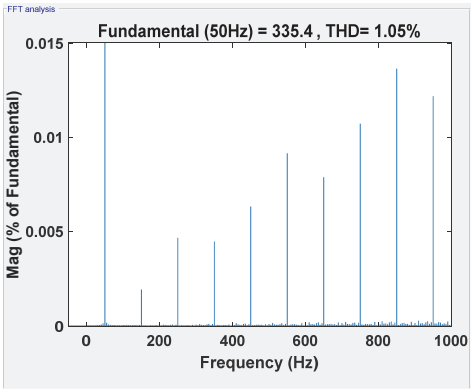

(c)

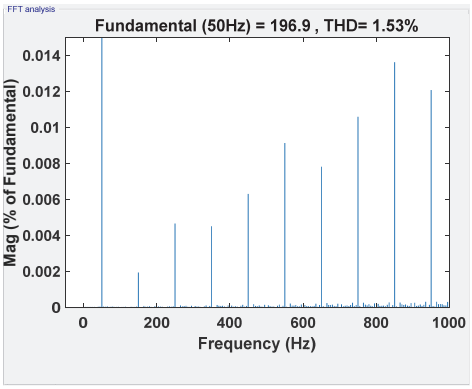

(d)

Figure 8 Operation of MALO based SAPF with PUC5 inverter (a) VSabc; (b) ISabc; (c) THDV; (d) THDi

Fig. 8 shows the efficiency of the proposed PUC5 inverter in SAPF with the proposed MALO, as well as an enhancement in the current shape and a significant reduction in THD in both voltage and current. The THD_V and THDi of the suggested PUC5 inverter are 1.05% and 1.53%, correspondingly, in relation to PSO in SAPF. A comparison of the two controllers' respective performances in the SAPF systems under study is given in Tab. 3 and Fig. 9.

Table 3 Comparative performance of PSO and MALO in PUC5 inverter based SAPF

% of THD	Controller	
	PSO	MALO
THD_V	1.21	1.05
THD_i	1.98	1.53

From the Tab. 3 and Fig. 9, it is clear Voltage THD is 1.21% and 1.05% by PSO and proposed MALO DC link controller in PUC5 inverter based SAPF respectively. Current THD is 1.98% and 1.53% by PSO and proposed MALO DC link controller in PUC5 inverter based SAPF correspondingly. This table shows that, in comparison to other systems, the harmonic mitigation in source voltage and current by the proposed MALO DC link controlled PUC5 inverter based SAPF is high. Both optimisers based SAPF reduce THD within IEEE standard 519 in comparison to the uncompensated system's current THD of 47.12%.

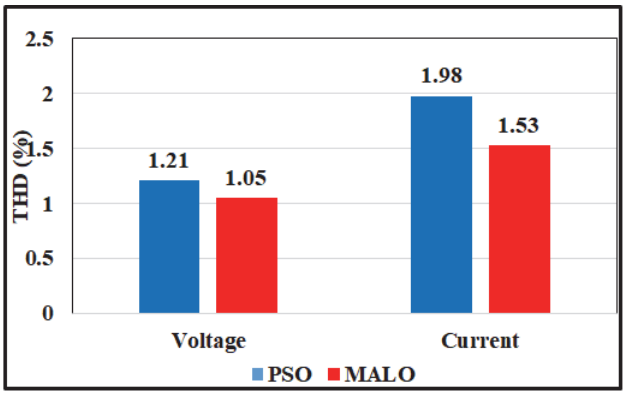

Figure 9 Operation of MALO based SAPF with PUC5 inverter (a) VSabc; (b) ISabc; (c) THDV; (d) THDi

To authenticate the effectiveness of the proposed system, it is related with existing articles with other optimization algorithms based SAPF for harmonic mitigation. Literature with SAPF using optimisation with balance nonlinear load is considered for comparison. State of the art of the proposed system in harmonic mitigation compared to without compensation is presented in Tab. 4.

Table 4 State of art of proposed system in harmonic mitigation

SAPF Controller Algorithm	THD without compensation in / %	THDi / %	THD mitigation compared to without compensation / %
Proposed MALO	47.12	1.53	96.75
FO [20]	11.4427	1.9316	83.12
HSO [20]	11.4427	2.2312	80.5
PPFO[20]	11.4427	1.9092	83.32
ACO [26]	28.01	3.72	86.72
BF [26]	28.01	3.71	86.75
GWO [22]	24.56	3.815	84.47
ALO [22]	24.56	1.4	94.3

From the Tab. 4 it is observed that PSO results minimized THD compared to HSO algorithm, while FO algorithm offered better performance than PSO based SAPF. Proposed MALO offered better harmonic mitigation compared to all other algorithms. From the comparison table it is observed that the proposed MALO controlled PUC5 based SAPF offered maximum harmonic mitigation, around 96.75%, compared with all other algorithms.

5 CONCLUSION

SAPF analysis is performed in this article to examine the enhancement of power quality in grid-connected PV-powered EV charging stations. An active power filter is required because several EV charging sessions introduce unpredictable harmonics into a grid. The SAPF's inverter is essential to the creation of the harmonic compensation signal. This paper analyses the SAPF based on PUC5

inverters for harmonic mitigation. Using modified pq theory for harmonic extraction, all Matlab/Simulink configuration inverters based on SAPF are utilised. Modified Antlion optimisation algorithm tuned PI controlled is proposed for DC voltage regulation in SAPF to enrich performance of filter. To authenticate effectiveness of proposed system it is compared with PSO based DC link controlled SAPF with PUC5 inverter. According to the analysis, THD without SAPF is as high as 47.12%. Within the IEEE standard, harmonic is decreased in both algorithms-based SAPF. The suggested MALO-based SAPF reduces current THD by about 0.45% in comparison to PSO SAPF. Maximum harmonic mitigation is achieved by the proposed MALO controlled PUC5 inverter-based SAPF when compared to PSO. The effectiveness of proposed system is revealed by comparison with existing articles with other optimization algorithms such as Firefly optimization algorithm and Harmony search optimization algorithm based SAPF. The research conducted provides a thorough examination of the proposed MALO controlled PUC5 inverter-based SAPF, revealing its ability to improve power quality through the execution of enhanced harmonic reduction using an adequate number of switching devices. In this article performance of the proposed system is verified by simulation analysis using Matlab/ Simulink. In the future it may extend with hardware implementation.

6 REFERENCES

[1] Singh, S., Saket, R. K., & Khan, B. (2023). A comprehensive state-of-the-art review on reliability assessment and charging methodologies of grid-integrated electric vehicles. *IET Electrical Systems in Transportation*, *13*(1), e12073. https://doi.org/10.1049/els2.12073

[2] Inci, M., Çelik, Ö., Lashab, A., Bayındır, K. Ç., Vasquez, J. C., & Guerrero, J. M. (2024). Power system integration of electric vehicles: A review on impacts and contributions to the smart grid. *Applied Sciences*, *14*(6), 2246. https://doi.org/10.3390/app14062246

[3] Mazza, A., Benedetto, G., Bompard, E., Nobile, C., Pons, E., Tosco, P., Zampolli, M., & Jaboeuf, R. (2023). Interaction among multiple electric vehicle chargers: Measurements on harmonics and power quality issues. *Energies*, *16*(20), 7051. https://doi.org/10.3390/en16207051

[4] Karthikeyan, M., Sharmilee, K., Balasubramaniam, P. M., Prakash, N. B., Babu, M. R., Subramaniyaswamy, V., & Sudhakar, S. (2020). Design and implementation of ANN-based shunt active power filter approach for current harmonics mitigation in industrial power systems. *Microprocessors and Microsystems*, *77*, 103194. https://doi.org/10.1016/j.micpro.2020.103194

[5] Mahmoud, M. O., Mamdouh, W., & Khalil, H. (2020). Source current harmonic mitigation of distorted voltage source by using shunt active power filter. *International Journal of Electrical and Computer Engineering*, *10*(4), 3967-3977. https://doi.org/10.11591/ijece.v10i4.pp3967-3977

[6] Choudhury, S., Bajaj, M., Dash, T., Kamel, S., & Jurado, F. (2021). Multilevel inverter: A survey on classical and advanced topologies, control schemes, applications to power system and future prospects. *Energies*, *14*(18), 5773. https://doi.org/10.3390/en14185773

[7] Rao, B. N., Suresh, Y., Panda, A. K., Naik, B. S., & Jammala, V. (2020). Development of cascaded multilevel inverter based active power filter with reduced transformers. *CPSS Transactions on Power Electronics and Applications*, *5*(2), 147-157. https://doi.org/10.24295/CPSSTPEA.2020.00015

[8] Tounsi, M. M., Allali, A., Boulouiha, H. M., & Denaï, M. (2021). ANFIS control of a shunt active filter with a five-level NPC inverter to improve power quality. *International Journal of Electrical and Computer Engineering*, *11*(3), 1886-1893. https://doi.org/10.11591/ijece.v11i3.pp1886-1893

[9] Chavali, R. V., Dey, A., & Das, B. (2021). A hysteresis current controller PWM scheme applied to three-level NPC inverter for distributed generation interface. *IEEE Transactions on Power Electronics*, *37*(2), 1486-1495. https://doi.org/10.1109/TPEL.2021.3052295

[10] Saleh, K. & Mahmoud, O. (2021). Asymmetrical four-wire cascaded H-bridge multilevel inverter based shunt active power filter supplied by a photovoltaic source. *International Journal of Power Electronics and Drive System*s, *12*(3), 1673-1681. https://doi.org/10.11591/ijpeds.v12.i3.pp1673-1681

[11] Vahedi, H., Shojaei, A. A., Dessaint, L. A., & Al-Haddad, K. (2017). Reduced DC-link voltage active power filter using modified PUC5 converter. *IEEE Transactions on Power Electronics*, *33*(2), 943-947. https://doi.org/10.1109/TPEL.2017.2674804

[12] Ali, M., Tariq, M., Lodi, K. A., Chakrabortty, R. K., Ryan, M. J., Alamri, B., & Bharatiraja, C. (2021). Robust ANN-based control of modified PUC-5 inverter for solar PV applications. *IEEE Transactions on Industry Applications*, *57*(4), 3863-3876. https://doi.org/10.1109/TIA.2021.3062081

[13] Amini, B., Rastegar, H., & Pichan, M. (2024). An optimized proportional resonant current controller based genetic algorithm for enhancing shunt active power filter performance. *International Journal of Electrical Power & Energy Systems*, *156*, 109738. https://doi.org/10.1016/j.ijepes.2023.109738

[14] Kumar, R., Bansal, H. O., Gautam, A. R., Mahela, O. P., & Khan, B. (2022). Experimental investigations on particle swarm optimization based control algorithm for shunt active power filter to enhance electric power quality. *IEEE Access*, *10*, 54878-54890. https://doi.org/10.1109/ACCESS.2022.3183565

[15] El-Saady, G., El-Sayed, A. H., Essamudin, A. E., & Abdul-Ghaffar, H. I. (2015). Harmonic compensation using online bacterial foraging optimization based three-phase active power filter. *WSEAS Transactions on Power Systems*, *10*, 73-81.

[16] Duc, M. L., Hlavaty, L., Bilik, P., & Martinek, R. (2023). Harmonic mitigation using meta-heuristic optimization for shunt adaptive power filters: A review. *Energies*, *16*(10), 3998. https://doi.org/10.3390/en16103998

[17] Rameshkumar, K. & Indragandhi, V. (2020). Real time implementation and analysis of enhanced artificial bee colony algorithm optimized PI control algorithm for single phase shunt active power filter. *Journal of Electrical Engineering & Technology*, *15*(6), 1541-1554. https://doi.org/10.1007/s42835-020-00430-2

[18] Bharathi, S. L. K. & Selvaperumal, S. (2020). MGWO-PI controller for enhanced power flow compensation using unified power quality conditioner in wind turbine squirrel cage induction generator. *Microprocessors and Microsystems*, *76*, 103080. https://doi.org/10.1016/j.micpro.2020.103080

[19] Kumar, R., Bansal, H. O., & Kumar, D. (2020). Improving power quality and load profile using PV-battery-SAPF system with metaheuristic tuning and its HIL validation. *International Transactions on Electrical Energy Systems*, *30*(5), e12335. https://doi.org/10.1002/2050-7038.12335

[20] Mahaboob, S., Ajithan, S. K., & Jayaraman, S. (2019). Optimal design of shunt active power filter for power quality enhancement using predator-prey based firefly optimization. *Swarm and evolutionary computation*, *44*, 522-533. https://doi.org/10.1016/j.swevo.2018.06.008

[21] Mirjalili, S. (2015). The ant lion optimizer. *Advances in Engineering Software*, *83*, 80-98. https://doi.org/10.1016/j.advengsoft.2015.01.010
[22] Bekakra, Y., Zellouma, L., & Malik, O. (2021). Improved predictive direct power control of shunt active power filter using GWO and ALO–Simulation and experimental study. *Ain Shams Engineering Journal*, *12*(4), 3859-3877. https://doi.org/10.1016/j.asej.2021.04.028
[23] El Bakrawy, L. M., Cifci, M. A., Kausar, S., Hussain, S., Islam, M. A., Alatas, B., & Desuky, A. S. (2022). A modified ant lion optimization method and its application for instance reduction problem in balanced and imbalanced data. *Axioms*, *11*(3), 95. https://doi.org/10.3390/axioms11030095
[24] Li, D., Wang, T., Pan, W., Ding, X., & Gong, J. (2021). A comprehensive review of improving power quality using active power filters. *Electric Power Systems Research*, *199*, 107389. https://doi.org/10.1016/j.epsr.2021.107389
[25] Shami, T. M., El-Saleh, A. A., Alswaitti, M., Al-Tashi, Q., Summakieh, M. A., & Mirjalili, S. (2022). Particle swarm optimization: A comprehensive survey. *IEEE Access*, *10*, 10031-10061. https://doi.org/10.1109/ACCESS.2022.3146702
[26] Sakthivel, A., Vijayakumar, P., Senthilkumar, A., Lakshminarasimman, L., & Paramasivam, S. (2015). Experimental investigations on ant colony optimized PI control algorithm for shunt active power filter to improve power quality. *Control Engineering Practice*, *42*, 153-169. https://doi.org/10.1016/j.conengprac.2015.04.013

Contact information:

S. RAMYA, Assistant Professor
(Corresponding author)
Department of EEE,
Karpagam Institute of Technology,
Coimbatore, India
E-mail: ramyas14101985@outlook.com

Dr. G. SUNDAR, Professor
Department of EEE,
Sri Shakthi Institute of Engineering and Technology,
Coimbatore, India
E-mail: Sund_geee@yahoo.co.in